
Wavelet-Based Image Tokenizer for Vision Transformers

Zhenhai Zhu
Google DeepMind
zhenhai@google.com

Radu Soricut
Google DeepMind
rsoricut@google.com

Abstract

Non-overlapping patch-wise convolution is the default image tokenizer for all state-of-the-art vision Transformer (ViT) models. Even though many ViT variants have been proposed to improve its efficiency and accuracy, little research on improving the image tokenizer itself has been reported in the literature. In this paper, we propose a new image tokenizer based on wavelet transformation. We show that ViT models with the new tokenizer achieve both higher training throughput and better top-1 precision for the ImageNet validation set. We present a theoretical analysis on why the proposed tokenizer improves the training throughput without any change to ViT model architecture. Our analysis suggests that the new tokenizer can effectively handle high-resolution images and is naturally resistant to adversarial attack. Furthermore, the proposed image tokenizer offers a fresh perspective on important new research directions for ViT-based model design, such as image tokens on a non-uniform grid for image understanding.

1 Introduction

Natural languages inherently use a discrete set of characters or bytes in a fixed alphabet. A sequence of bytes can be directly treated as the input to a Transformer model [56], as done in ByT5 [59]. However, the latent representations for such byte sequences may not carry enough information, and the sequence length could be unnecessarily long. A more common alternative is segmenting words into subword tokens either explicitly [30, 46] or implicitly [51]. The explicit subword tokenizer has been a default component in many state-of-the-art (SOTA) large language models such as T5 [39], GPT3 [6], ULM [50], PaLM [10] and Chinchilla [26].

Image pixels are also discrete since the RGB channels are represented by 8-bit unsigned integers. This means that the raw pixel vocabulary size is 2^{24} , too large to be practical. In addition, the sequence length for an image with even a moderate resolution of 256×256 is too long. A commonly used image tokenizer for the vision Transformer (ViT) [17] is the non-overlapping patch-wise convolution. Despite many variants of ViT [55, 53, 32, 5, 31], this patch-convolution based tokenizer is still the default choice for SOTA ViT models [47, 65, 16]. Since ViT models are the image encoders in the largest vision-language models such as CLIP [38], ALIGN [27], CoCa [63] and PaLI [8], the patch-convolution based image tokenizer becomes a default component in these vision-language models.

An image tokenizer performs two main tasks: 1) it partitions a given image into non-overlapping patches so that the final token count is considerably smaller than the image pixel count; 2) it maps the RGB channels for the pixels in each patch into a token embedding vector. This converts a set of image patches to an input token sequence. The image tokenizer inevitably removes the relative position information among the pixels associated with each image token. A good image tokenizer must therefore strike a balance between the loss in position information and the savings in compute, both due to token-count reduction. At the same time, different vision tasks have different require-

ments for these two conflicting aspects. For datasets with high-resolution images [34, 31], token count can easily become the bottleneck due to the quadratic complexity of the standard Transformer attention [49]. For vision tasks like semantic segmentation [11, 67] and object detection [20, 21], the relative position or spatial information in general plays a crucial role. We believe that a good tokenizer should effectively compress the redundant information in patch pixels. This allows the flexibility to accommodate the two conflicting requirements, and has motivated us to look into the image compression field for inspiration.

There are many well-established and well-understood algorithms in the image compression field [23]. The central goal in image compression is to remove redundant information in pixel space such that the reconstructed images are visually close to the original images. The prevailing algorithm used in current industry standard JPEG2000 [1] is the wavelet transformation [15, 48].

In this paper, we draw inspiration from the crucial insight in JPEG2000: most high-frequency signals revealed by the wavelet transformation can be safely truncated with minimal human perception difference. This is where the bulk of the image compression occurs. In short, we propose to replace the patch-convolution-based image tokenizer in the standard ViT architecture [17] with a wavelets-based image tokenizer.

Our main **contributions** are:

1. We introduce a new concept called pixel-space token embedding and show how to use wavelet transformation to compute it (Section 4.1). The pixel-space token embedding is naturally resistant to adversarial attacks and its sparsity can be used to produce image tokens on a non-uniform grid.
2. We present a theoretical analysis on how to use a block sparse projection to map truncated pixel-space token embeddings to semantic token embeddings with reduced dimensions (Section 4.2). This is important for training ViT models on datasets with images at higher resolutions.
3. The wavelet-based tokenizer offers an elegant solution to alleviating the computational impact of the two quadratic terms in Transformer layer op counts (Section 4.3). To the best of our knowledge, efficient Transformer research primarily focuses on the quadratic term $O(T^2)$, where T is token count (sequence length). For some tasks and datasets, however, the op count is actually dominated by the other quadratic term $O(H^2)$, where H is embedding size. Our new image tokenizer provides an efficient handle on this.
4. We use empirical evidence to show that ViT models with the proposed wavelet-based tokenizer achieve higher training throughput and better top-1 precision (on the ImageNet val set, see Section 5), while reducing the overall model size.

2 Related Work

The information redundancy in images has been previously exploited in the design of ViT variants. For instance, less informative patch-wise image tokens are omitted in later-stage of an adaptive ViT [61] or merged into tokens with larger but lower-resolution patches [41]. These approaches are less straightforward compared to ours, as they involve modification of ViT model, loss function and training recipe. Our wavelets-base tokenizer offers a more principled framework to achieve the same goal, and it comes with a drop-in replacement of only the convolution-based tokenizer and no further changes. We will come back to this in section 4.1.

Wavelet transformation has been used as a lossless up-sampling and down-sampling technique in ViT [60]. This approach is tangent to the image tokenizer proposed and studied in this paper.

JPEG-inspired algorithms have been proposed for image generation [36], where the discrete cosine transformation (DCT) coefficients are directly generated by an autoregressive Transformer decoder. The sequence length is still a severe limiting factor, to the extent to which only low-resolution images can be generated. In our initial experiments, we used DCT as a building block for the image tokenizer, but the results were inferior to those obtained with wavelet-based image tokenizers.

Earlier image generation work directly decodes pixel RGB channels and can only generate low-resolution images [7, 37]. Current SOTA text-to-image autoregressive generation models such as DALL-E [40] and others [62] all use a two-stage approach. The first stage trains an image tokenizer and detokenizer with a codebook of discrete visual tokens. The second stage trains a Transformer model that generates the final images from text prompts. The backbone in the tokenizers is either

the discrete variational autoencoder (dVAE) [54] in DALL-E [40] or ViT-based VQGAN [18] (ViT-VQGAN) in [62]. They also often involve vector quantization in order to generate discrete visual tokens. Standard ViT models do not need a codebook with discrete tokens. Hence the tokenizers in [40, 18, 62] are outside the scope of this paper. However, the convolutional neural network (CNN) based image encoder used by VQGAN in [18] or dVAE in DALL-E [40] is related to our work because it has been recognized that the lower-level convolutional kernels in CNNs are very similar to Gabor wavelet filters [33, 57]. This area requires further investigation into connecting these approaches.

3 A Brief Introduction to Wavelet-Based Image Compression

We first describe the discrete wavelet transformation in terms of convolution kernels. We refer the readers to excellent books such as [15, 48] for a comprehensive review of the theory on wavelet transformation.

A color image with resolution $N \times N$ and RGB channels can be represented by a tensor $P \in R^{N \times N \times 3}$. It is common practice in image compression to convert the RGB format to the luminance-chrominance format via a fixed and invertable linear projection [23]. This is represented by another tensor $[Y, C_b, C_r] \in R^{N \times N \times 3}$ where $Y \in R^{N \times N}$ is the luminance matrix, and $C_b, C_r \in R^{N \times N}$ are the chrominance-blue and chrominance-red matrix, respectively. It is known that human visual perception is more sensitive to the brightness or luminance and less sensitive to the color or chrominance [23]. Hence it is common practice to reduce the original image resolution for C_b and C_r by a factor of 2×2 before the wavelet transformation is applied. This reduces the overall pixel count by a factor of 2.

There are many families of wavelets. Here we focus on two families that are effective for the purpose of image tokenizer: Daubechies (db) and Coiflets (coif). One can choose different orders within each family. For instance, the lowest-order one-dimensional (1D) kernels in db and coif families are, respectively, the db1 (also called Haar) kernels:

$$K_l = \begin{bmatrix} \frac{1}{\sqrt{2}} & \frac{1}{\sqrt{2}} \end{bmatrix}, \quad K_h = \begin{bmatrix} \frac{1}{\sqrt{2}} & -\frac{1}{\sqrt{2}} \end{bmatrix} \quad (1)$$

and the coif1 kernels:

$$\begin{bmatrix} K_l \\ K_h \end{bmatrix} = \begin{bmatrix} -0.016 & -0.073 & 0.385 & 0.853 & 0.338 & -0.073 \\ 0.073 & 0.338 & -0.853 & 0.385 & 0.073 & -0.016 \end{bmatrix}. \quad (2)$$

The two-dimensional (2D) kernels are derived from 1D kernels as

$$K_{ll} = K_l^T K_l, \quad K_{lh} = K_l^T K_h, \quad K_{hl} = K_h^T K_l, \quad K_{hh} = K_h^T K_h. \quad (3)$$

The convolution with these four 2D kernels is then performed on Y , C_b and C_r separately. This is also known as the group convolution. For instance, convolution on matrix Y results in

$$Y^{(1)} = \mathbf{conv}_{2d}(K_{ll})(Y^{(0)}), \quad Y_h^{(1)} = \mathbf{conv}_{2d}(K_{lh})(Y^{(0)}) \quad (4)$$

$$Y_v^{(1)} = \mathbf{conv}_{2d}(K_{hl})(Y^{(0)}), \quad Y_d^{(1)} = \mathbf{conv}_{2d}(K_{hh})(Y^{(0)}) \quad (5)$$

where $Y^{(0)} = Y$ and $\mathbf{conv}_{2d}(M)$ is the 2D convolution with kernel M and a fixed stride (2, 2). The same convolution in equations (4)-(5) can be recursively performed on matrix $Y^{(k)}$ for $k = 1, 2, \dots$. The stride (2, 2) dictates that each recursion step reduces the image resolution by a factor of 2×2 . Matrices $Y^{(k)}$, $Y_h^{(k)}$, $Y_v^{(k)}$ and $Y_d^{(k)}$ can be gathered into a single matrix. For instance, a simple level-2 wavelet transformation on matrix Y results in

$$\left[\begin{array}{cc|c} Y^{(2)} & Y_h^{(2)} & Y_h^{(1)} \\ Y_v^{(2)} & Y_d^{(2)} & \\ \hline Y_v^{(1)} & & Y_d^{(1)} \end{array} \right]. \quad (6)$$

The procedure in equations (4)-(6) is also applied to matrices C_b and C_r , and we obtain the same matrix structure shown in equation (6) for C_b and C_r .

Figure 1 shows a level-10 wavelet transformation using the db1 kernels of equation (1) on an image with YC_bC_r channels. Notice that majority of the wavelet coefficients are nearly zero. This is particularly true for channel- C_b and channel- C_r . This distribution is typical of a natural image and it gives us plenty of room to safely sparsify or zero out those near-to-zero wavelet coefficients with minimal quality loss in the reconstructed image. All non-zero coefficients are quantized and then compressed further with entropy coding algorithms. We refer interested readers to [1] for details on this step.

We can easily reverse the steps in equations (4)-(6) and reconstruct the original image. The main difference is that we need to use transposed convolution in equations (4)-(5).

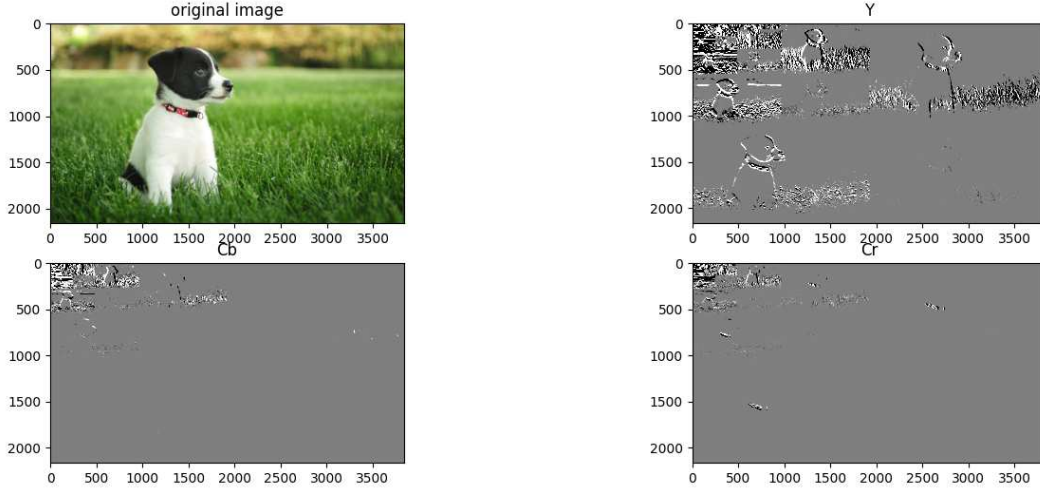


Figure 1: Original image and its wavelet coefficients for YC_bC_r channels, where black/white/grey dots correspond to strongly positive / strongly negative / near-to-zero coefficients, respectively.

4 Image Tokenizer

In this section, we depart from the image compression concepts behind the standard JPEG2000 algorithm and focus on designing an effective image tokenizer. The common goal is to remove redundant information in an image, hence wavelet transformation is a shared component. However, the end goals are different. In an image compression algorithm, each step must be reversible such that the original image can be reconstructed from JPEG strings with minimal visual-perception quality loss. On the other hand, an image tokenizer is designed to capture semantically meaningful information. The generated token embeddings serve as the starting point for the subsequent processing performed by ViT models, namely, the "echo chambers" effect in attention layers [25] and the key-value pair memories in feedforward layers [22].

4.1 Pixel-Space Token Embedding

Same as in JPEG2000, we adopt the RGB-to- YC_bC_r linear transformation and downsample C_b and C_r channels by a factor 2×2 . Hence for an image with resolution $N \times N$, the input to the wavelet transformation is YC_bC_r channels with shape $Y \in R^{N \times N}$ and $C_b, C_r \in R^{\frac{N}{2} \times \frac{N}{2}}$.

Unlike Fourier or discrete cosine transformation, wavelet transformation uses localized kernels, see equations (1) and (2). Therefore, each wavelet coefficient is related only to a local pixel region. We can illustrate this with a concrete example. Given a color image with resolution 128×128 , we follow the procedure in equations (4)-(5) and perform a level-2 wavelet transformation on YC_bC_r channels. We can re-write the resulting matrix in equation (6) and its counter parts for C_b and C_r

as:

$$P^{(2)} = \begin{bmatrix} Y^{(2)} & C_b^{(2)} & C_r^{(2)} \end{bmatrix} \quad (7)$$

$$D^{(2)} = \begin{bmatrix} Y_h^{(2)} & Y_v^{(2)} & Y_d^{(2)} & C_{bh}^{(2)} & C_{bv}^{(2)} & C_{bd}^{(2)} & C_{rh}^{(2)} & C_{rv}^{(2)} & C_{rd}^{(2)} \end{bmatrix} \quad (8)$$

$$D^{(1)} = \begin{bmatrix} Y_h^{(1)} & Y_v^{(1)} & Y_d^{(1)} \end{bmatrix} \quad (9)$$

where $P^{(2)} \in R^{32 \times 32 \times 3}$, $D^{(2)} \in R^{32 \times 32 \times 9}$ and $D^{(1)} \in R^{64 \times 64 \times 3}$. Note that we have skipped the convolution on C_b and C_r at resolution 128×128 since they are already downsampled to 64×64 . This is why there is no C_b or C_r component in equation (9). Note also that $P^{(2)}$ is just a coarsened image with YC_bC_r channels at resolution 32×32 . We can reshape tensor $D^{(1)}$ such that $D^{(1)} \in R^{32 \times 32 \times 12}$ and concatenate $P^{(2)}$, $D^{(2)}$ and $D^{(1)}$ along their last dimension into one tensor as

$$W = [P^{(2)} \quad D^{(2)} \quad D^{(1)}] = [W^{(2)} \quad W^{(1)}] \quad (10)$$

where $W \in R^{32 \times 32 \times 24}$, $W^{(2)} = [P^{(2)} \quad D^{(2)}] \in R^{32 \times 32 \times 12}$ and $W^{(1)} = D^{(1)}$. More generally, a level- L wavelet transformation on an image with resolution $N \times N$ results in a set of tensors concatenated along their last dimension as

$$W = [W^{(L)} \quad W^{(L-1)} \quad \dots \quad W^{(1)}] \quad (11)$$

where $W^{(k)} \in R^{\tilde{N} \times \tilde{N} \times C_k}$, $\tilde{N} = \frac{N}{2^L}$ and

$$C_k = \begin{cases} 12 & k = L \\ 9 \times 4^{L-k} & k = 2, \dots, L-1 \\ 3 \times 4^{L-1} & k = 1 \end{cases} \quad (12)$$

The number of entries in vector $W(i, j, :)$ in equation (11) is

$$C = \sum_{k=1}^L C_k = \frac{3}{2} 4^L. \quad (13)$$

We treat the length- C vector $W(i, j, :)$ as the pixel-space embedding for pixel- (i, j) in the coarse image with resolution $\tilde{N} \times \tilde{N}$. For the simple level-2 example in equation (10), we only need vector $W(i, j, :)$ with its 24 entries to reconstruct the 4×4 original pixel region corresponding to pixel- (i, j) in coarse image $P^{(2)}$. This can be done by following steps in equations (4)-(10) in reverse order. The same procedure also applies to the general case in equation (11). This reconstruction is exact if there is no truncation, i.e. no small wavelet coefficients are zeroed out. As shown in Fig 1, truncation via thresholding can be done easily. JPEG2000 has demonstrated that the reconstruction error is small even if more than 90% of the wavelet coefficients are zeroed out. Therefore, the pixel-space token embedding from this point on always refers to the post-truncation version of vector $W(i, j, :)$.

A few remarks are in order:

1. Token count in pixel-space embedding tensor W is $\tilde{N}^2 = \frac{N^2}{4^L}$. So level- L is used as a hyperparameter to achieve the trade-off between token count reduction and the loss of positional information, as discussed in Section 1.
2. Wavelet kernels are fixed, as shown in equations (1) and (2). So any gradient-based adversarial examples [24] would fail since there is no gradient with respect to these kernels. In general, any small white-noise-like perturbation to the input images becomes high-frequency wavelet coefficients [3, 52], which are zeroed out in the sparsification step. Therefore, a wavelet-based tokenizer is naturally resistant to adversarial attacks on image classifiers (e.g., [44]).
3. Wavelet transformation exposes image regions with smooth RGB pixels. The sparsity in each pixel-space embedding vector correlates strongly with the information entropy in the corresponding pixel region. This can be used as a useful signal in the design and implementation of the image tokenizer. For instance, it can be used to guide a non-uniform image partition, and produce image tokens on a non-uniform grid*. This is in spirit similar to the goal in [61, 41], but wavelet transformation provides a more principled framework. This involves modification to the ViT model itself and hence is outside the scope of this paper.

*The non-uniform grid or mesh is a standard technique in numerical methods for partial differential equations [45, 35]. It is an indispensable tool for handling large variance in variables such as electric potential or airflow pressure as a function of spatial coordinates. The RGB or YC_bC_r intensities in natural images also vary considerably with pixel coordinates.

4.2 Semantic Token Embedding

The goal of this next step is to map the pixel-space embeddings to semantically-meaningful token embeddings. This mapping can be a simple trainable linear projection

$$E = WQ \quad (14)$$

where $E \in R^{\tilde{N} \times \tilde{N} \times H}$ is the semantic token embedding tensor, H is the target embedding size, $Q \in R^{C \times H}$ is the trainable projection matrix, and $W \in R^{\tilde{N} \times \tilde{N} \times C}$ is defined in equation (11).

Equation (13) shows that pixel-space embedding size grows exponentially with the wavelet level L . However, each vector $W(i, j, :)$ in equation (11) is extremely sparse, with a predictable sparsity pattern. For the level-10 wavelets shown in Figure 1, nearly all entries in $W^{(1)}$ are zeros, whereas $W^{(L)}$ has almost no zero entries. In general, the proportion of zeros in $W^{(k)}$ grows rapidly, maybe exponentially, as level index k decreases. Our experiments (Tables 1-2) show that sparsifying 80% of the entries in W actually boosts the image classification top-1 precision. We believe the reason is that those small wavelet coefficients contain more noise than signal, and filtering them out serves as a form of regularization for model training.

We can use a block sparse structure in matrix Q to exploit this sparsity pattern. The new projection is

$$E = WQ = W \begin{bmatrix} Q^{(L)} & 0 & \dots & 0 \\ 0 & Q^{(L-1)} & \dots & 0 \\ \vdots & \vdots & \ddots & 0 \\ 0 & 0 & 0 & Q^{(1)} \end{bmatrix} \quad (15)$$

where $Q^{(k)} \in R^{C_k \times H_k}$, C_k is defined in equation (12), and H_k is the token embedding size assigned to level- k under the constraint

$$\sum_k H_k = H. \quad (16)$$

In view of equation (11), we have

$$E = [E^{(L)} \quad E^{(L-1)} \quad \dots \quad E^{(1)}] \quad (17)$$

where

$$E^{(k)} = W^{(k)} Q^{(k)}. \quad (18)$$

The key question is: what is a right value for H_k given C_k in equation (12)? This obviously depends on the sparsity of vector $W^{(k)}(i, j, :)$. For higher wavelet levels like $k = L$ or $k = L - 1$, tensor $W^{(k)}$ is dense and hence we can simply set $H_k = C_k$. It is the much larger projection matrix like $Q^{(1)}$ that makes a significant difference to the parameter count and runtime. Fortunately, tensor $W^{(1)}$ is very sparse and this offers a good opportunity to find a H_k much smaller than C_k .

To facilitate the exposition, we focus on the calculation of vector $E^{(k)}(i, j, :)$

$$E^{(k)}(i, j, :) = e_{ij}^T = W^{(k)}(i, j, :) Q^{(k)} = w_{ij}^T Q^{(k)} \quad (19)$$

or equivalently

$$e_{ij} = (Q^{(k)})^T w_{ij} \quad (20)$$

where $e_{ij} \in R^{H_k \times 1}$, $w_{ij} \in R^{C_k \times 1}$, and $(Q^{(k)})^T \in R^{H_k \times C_k}$. Note that the positions of nonzero entries in vector w_{ij} are random, depending on the image being processed. We show in two steps that we could set H_k to the expected numerical rank of matrix $Q^{(k)}$, which is much smaller than C_k for small k . The first step can be formalized as the following proposition:

Proposition 1 For a linear projection

$$\vec{y} = A\vec{x} \quad (21)$$

where $A \in R^{M \times N}$, $\vec{x} \in R^N$ and only a random subset of entries in \vec{x} are nonzero. The probability of an entry in \vec{x} being nonzero is p . Suppose we sample such a Bernoulli distribution to generate a random \vec{x} and accumulate the resulting \vec{y} into a matrix

$$B = [\vec{y}_1, \vec{y}_2, \dots], \quad (22)$$

then the expected column rank of B is pN .

Proof: Column rank of A is N , but only pN of them are used to compute each \vec{y}_i . So the columns of matrix B can only span a space covered pN columns of matrix A in probability. This is the expected column rank of matrix B . \square

Suppose we collect all embedding vectors e_{ij} in equation (20) into a single matrix S . Let the total token count be S_t and hence $S \in R^{H_k \times S_t}$. Note that S_t could be a huge number since matrix S includes every level- k pixel-space embedding vector in tensor $W^{(k)}$ extracted from all images in the training dataset. So obviously $H_k \ll S_t$. The second step can be stated as the next proposition.

Proposition 2 The expected numerical rank of matrix S is $\min(H_k, pC_k)$.

Proof: In view of equation (20) and (21), we can see that e_{ij} corresponds to y and w_{ij} corresponds to x . Likewise, matrix S corresponds to B in equation (22). As a direct result from Proposition-1, the expected column rank of matrix S is pC_k . Hence $\text{rank}(S) = \min(H_k, pC_k)$. \square

Since we have the flexibility to set H_k such that the information in w_{ij} is preserved in e_{ij} after the projection in equation (20), we can simply set $H_k = pC_k$. Even though C_k in equation (12) can be large for small k such as $k = 1$, empirically we see that probability p is very small for small k . This means that $H_k = pC_k$ is nearly constant for small k . For large k such as $k = L$, we set $H_k = C_k$ since the pixel-space embeddings are fully dense or equivalently $p = 1$. In view of equation (16), the semantic token embedding size H is close to an affine function instead of an exponential function in wavelet level L .

Consider an image with resolution $N \times N$, patch-convolution based tokenizer with patch size $p \times p$ generates $T = \frac{N^2}{p^2}$ tokens. Patch convolution becomes ineffective at extracting visual information when p is too large, which is why $p = 8, 16, 32$ are common choices. Hence the operation count for the standard ViT with patch-convolution tokenizer grows as $O(T^2) = O(\frac{N^4}{p^4})$. This becomes prohibitively expensive when $N > 2048$. However, this high image resolution can be reduced to a user-specified resolution $\tilde{N} = \frac{N}{2^L}$ with a level- L wavelet-based tokenizer, where $L = \log_2(\frac{N}{\tilde{N}})$. Since semantic token embedding size H in equation (16) is affine in L , as discussed above, we have $H = O(\log_2(\frac{N}{\tilde{N}}))$ which grows slowly with N . Therefore, wavelet-based tokenizer offers a much more efficient way to handle high image resolution due to the block sparse projection in equation (15).

We could add more dense layers on top of the single linear layer in equation (15) to potentially improve the token embedding quality. The increase in parameter count and training cost due to the added layers is $O(H^2)$. This is much smaller than $O(CH)$ in equation (15) since the embedding dimension has been reduced from a large C in equation (13) to a small H in equation (16).

4.3 Operation Count For Transformer Layers

A standard Transformer consists of many identical layers with the following hyper parameters: token embedding size H , model hidden state size which is typically the same H , attention query, key and value feature size d_{model} which is typically also the same H , and feed-forward intermediate layer activation size $d_{ff} = m \times H$ (with integer m typically in the range $[2, 10]$). As before, let T be the token count. The breakdown of the operation count for each Transformer layer is

- Attention: $2T^2H + 4TH^2$
 - Query/Key/Value multihead projections and output projection: $4TH^2$
 - Query Key inner-product and Attention Value multiplication: $2T^2H$
- Feedforward: $2mTH^2$

We focus our attention on the two quadratic terms: $2T^2H$ and $(2m + 4)TH^2$. If we use a typical $m = 4$, then the ratio between them is

$$r = \frac{2T^2H}{(2 \times 4 + 4)TH^2} = \frac{T}{6H}. \quad (23)$$

Much of the efficient Transformer research focuses on improving the $O(T^2)$ quadratic complexity in Transformer attention [49, 68, 42, 9, 58, 29, 64, 2, 4]. This is important for tasks with long-context

such as long-document summarization and long-video understanding and generation because $T \gg H$ and hence $r \gg 1$ in equation (23). However, the other quadratic term $O(H^2)$ dominates for many standard language or vision models and datasets. For example, $T = 512, H = 1024$ are used in a T5-large model [39], and $T = 256, H = 4096$ are used in ViT image encoder in SOTA vision-language model PaLI [8]. In such cases, $r \ll 1$ in equation (23) and hence it is more cost-effective to reduce H using the wavelet-base image tokenizer with the block sparse projection from Section 4.2. In Section 5 we confirm empirically that this is exactly what is observed for ViT models.

We should note that matrix-tiling and operation-fusion idea in the recently proposed Flash Attention [13, 14] has essentially removed the quadratic memory complexity for Transformer models. So we do not include memory usage in our analysis. The discussion here only focus on the forward path in model training. The analysis for the backward gradient propagation path follows the same reasoning and the same conclusion applies.

5 Experimental Results

5.1 Setup

Dataset We use the ILSVRC-2012 ImageNet dataset with 1k classes and 1.3M images [43]. The image resolution has two settings: 256×256 and 512×512 .

ViT Models Our baseline model is the ViT-base model in [17] with the same model parameters: $H = d_{model} = 768, d_{ff} = 3072, 12$ Transformer layers, 12 attention heads. We treat d_{model} and H as two independent hyper parameters so we can check their separate effects on training throughput and top-1 precision. All models are trained on TPUs v4 [19, 28] with the same training hyper parameters reported in [17], such as batch size, epochs, learning rate, weight decay and etc. We follow the data augmentation recipe in [47] which uses the combination of Mixup [66] and RandAugment [12]. The results below clearly show that wavelet-based tokenizer does not interfere with these data augmentation tricks. We want to emphasize that ViT model architecture and training recipe are held unchanged as we do a drop-in replacement of patch-convolution image tokenizer with our wavelet-based tokenizer. This way, the improvement can directly be attributed to the wavelet tokenizer.

Patch-convolution tokenizer variants are controlled by patch size only. We use the notations patch/8, patch/16 and patch/32 in table 1 and table 2 to denote these variants. For instance, patch/8 means that a 8×8 pixel region corresponds to one ViT input token.

Wavelet-based tokenizer variants are controlled by two groups of parameters:

1) The wavelet transformation parameters include wavelet type and level- L , as well as the percentage of wavelet coefficients to be zeroed out with thresholding. We use the notations db1-4 and db1-5 for level-4 and level-5 wavelet transformations, respectively, with the db1 kernels defined in equation (1). Similarly, coif1-3 and coif1-4 refer to level-3 and level-4 wavelet transformations, respectively, with the coif1 kernels defined in equation (2). By default, 80% of the wavelet coefficients of W in equation (11) are zeroed out. This percentage is appropriate for image resolutions 256×256 and 512×512 (it should be higher for higher-resolution images).

2) The dense projection parameters include H_k in equation (16) and number of additional dense layers. As discussed in section 4.2, we set $H_k = C_k$ for $k = L, L - 1$. We perform hyper parameter sweep for H_1 such that the top-1 precision is optimized under the constraint that H in equation (16) is an integer multiple of 128. Two top performing choices ($H = 256, 384$) and their impact are shown in Table 3. Our experiments show that one additional dense layer does not bring any gain in top-1 precision. This is likely due to the fact that L is only up to 5 for image resolution 512×512 . We believe more dense layers will be needed for resolution higher than 1024×1024 .

Input sequence length It should be noted that each wavelet-based token corresponds to a pixel region with size $2^L \times 2^L$ in the original image. So the input sequence generated from an image with resolution 256×256 by coif1-3 and patch/8 have the same length $(\frac{256}{8})^2 = 32^2 = 1024$. This sequence length is denoted as *tokens* in all result tables.

5.2 Tokenizer Comparison

We run experiments comparing patch-convolution-based tokenizers (denoted as patch/ N , where N is the patch size) versus wavelet-based tokenizers (db and coif). We report results on images with resolutions 256×256 (Table 1) and 512×512 (Table 2). The training is done using TPUv4 accelerators, and throughput is measured in number of images per second per TPU core. The results show that the wavelet-based tokenizers have both better top-1 precision and higher training throughput. Remarkably, wavelet-based tokenizers also reduce model parameter count significantly because H is reduced, due to the block sparse projection in equation (15).

Table 1: Top-1 precision and throughput (plus stats) for ImageNet-1K (val set), 256x256 image resolution; patch/8,16 are patch-convolution tokenizers, coif1-3 and db1-4 are wavelet tokenizers.

tokenizer	prec@top-1 (\uparrow)	throughput (\uparrow)	params (M) (\downarrow)	tokens	H	d_{model}	d_{ff}
patch/8	82.21	99.8	86.76	1024	768	768	3072
coif1-3	83.43 $+1.22$	116.5 $+17\%$	44.05 $+49\%$	1024	384	768	3072
patch/16	80.30	589	86.61	256	768	768	3072
db1-4	81.56 $+1.26$	996 $+69\%$	43.87 $+49\%$	256	384	768	3072

Table 2: Top-1 precision and throughput (plus stats) for ImageNet-1K (val set), 512x512 image resolution; patch/16,32 are patch-convolution tokenizers, coif1-4 and db1-5 are wavelet tokenizers.

tokenizer	prec@top-1 (\uparrow)	throughput (\uparrow)	params (M) (\downarrow)	tokens	H	d_{model}	d_{ff}
patch/16	82.86	99.8	87.2	1024	768	768	3072
coif1-4	83.14 $+0.28$	102.1 $+2\%$	44.31 $+49\%$	1024	384	768	3072
patch/32	80.89	311	88.38	256	768	768	3072
db1-5	81.63 $+0.74$	341 $+10\%$	59.59 $+33\%$	256	512	768	3072

5.3 Effect of Token Embedding Sizes

We report the results of using different H , d_{ff} and d_{model} in Table 3. Smaller H allows us to make some useful trade-off. For instance, configuration $H = 384$, $d_{model} = 768$ means that the multihead projection size is down by $\frac{1}{2}$ and the feedforward layer size is down by a factor of $\frac{3}{4}$. This saving allows us to enlarge d_{ff} from $4 \times H$ to up to $16 \times H$. This flexibility allows the trade-off between precision and training throughput, as shown in Table 3.

Table 3: Study on the effect of different H , d_{ff} and d_{model} on Top-1 precision for ImageNet-1K (val set) and training throughput, 256x256 image resolution.

tokenizer	tokens	prec@top-1 (\uparrow)	throughput (\uparrow)	params (M)	d_{model}	H	d_{ff}
db1-4	256	79.44	1422	14.21	256	256	3072
db1-4	256	80.44	1101	29.52	768	256	3072
db1-4	256	81.12	864	48.43	768	256	6144
db1-4	256	81.22	1052	36.77	384	384	3072
db1-4	256	81.56	996	43.87	768	384	3072
db1-4	256	81.55	769	72.21	768	384	6144

6 Conclusions And Future Work

We describe a new wavelet-based image tokenizer as a drop-in replacement for the patch-convolution based tokenizer used in the standard ViT models. We demonstrate that ViT models equipped with the new tokenizer achieve both higher training throughput and better top-1 precision for the ImageNet validation set. We also present a theoretical analysis on why the proposed tokenizer improves the training throughput, without any change to the ViT model architecture. Our analysis also indicates that the new tokenizer can effectively handle high-resolution images and is naturally resistant to adversarial attacks. Overall, our image tokenizer offers a fresh perspective on important new research directions for ViT-based model design, such as image tokens on a non-uniform grid and a new approach to modeling increased resolution in images.

References

- [1] Tinku Acharya and Ping-Sing Tsai. *JPEG2000 Standard for Image Compression: Concepts, Algorithms and VLSI Architectures*. Wiley-Interscience, 2004.
- [2] Joshua Ainslie, S. Ontañón, C. Alberti, V. Cvicek, Zachary Kenneth Fisher, Philip Pham, Anirudh Ravula, S. Sanghai, Qifan Wang, and L. Yang. Etc: Encoding long and structured inputs in transformers. In *EMNLP*, 2020.
- [3] Fábio Mariano Bayer, Alice J. Kozakevicius, and Renato J. Cintra. An iterative wavelet threshold for signal denoising. *ArXiv*, abs/2307.10509, 2019.
- [4] Iz Beltagy, Matthew E. Peters, and Arman Cohan. Longformer: The long-document transformer. *ArXiv*, abs/2004.05150, 2020.
- [5] Lucas Beyer, Pavel Izmailov, Alexander Kolesnikov, Mathilde Caron, Simon Kornblith, Xiaohua Zhai, Matthias Minderer, Michael Tschannen, Ibrahim Alabdulmohsin, and Filip Pavetic. Flexivit: One model for all patch sizes. In *CVPR*, 2023.
- [6] Tom B. Brown, Benjamin Pickman Mann, Nick Ryder, Melanie Subbiah, Jean Kaplan, Prafulla Dhariwal, Arvind Neelakantan, Pranav Shyam, Girish Sastry, Amanda Askell, Sandhini Agarwal, Ariel Herbert-Voss, G. Krüger, Tom Henighan, Rewon Child, Aditya Ramesh, Daniel M. Ziegler, Jeffrey Wu, Clemens Winter, Christopher Hesse, Mark Chen, Eric J Sigler, Mateusz Litwin, Scott Gray, Benjamin Chess, Jack Clark, Christopher Berner, Sam McCandlish, Alec Radford, Ilya Sutskever, and Dario Amodei. Language models are few-shot learners. *ArXiv*, abs/2005.14165, 2020.
- [7] Mark Chen, Alec Radford, Rewon Child, Jeffrey Wu, Heewoo Jun, David Luan, and Ilya Sutskever. Generative pretraining from pixels. *Proceedings of the 37th International Conference on Machine Learning*, PMLR 119, 2020.
- [8] Xi Chen, Xiao Wang, Soravit Changpinyo, A. J. Piergiovanni, Piotr Padlewski, Daniel Salz, Sebastian Goodman, Adam Grycner, Basil Mustafa, Lucas Beyer, Alexander Kolesnikov, Joan Puigcerver, Nan Ding, Keran Rong, Hassan Akbari, Gaurav Mishra, Linting Xue, Ashish Thapliyal, James Bradbury, Weicheng Kuo, Mojtaba Seyedhosseini, Chao Jia, Burcu Karagol Ayan, Carlos Riquelme, Andreas Steiner, Anelia Angelova, Xiaohua Zhai, Neil Houlsby, and Radu Soricut. PaLI: A jointly-scaled multilingual language-image model. *arXiv preprint arXiv:2209.06794*, 2022.
- [9] Krzysztof Choromanski, Valerii Likhoshesterov, David Dohan, Xingyou Song, Jared Davis, Tamás Szilvassy, David Belanger, Lucy J. Colwell, and Adrian Weller. Masked language modeling for proteins via linearly scalable long-context transformers. *ArXiv*, abs/2006.03555, 2020.
- [10] Aakanksha Chowdhery, Sharan Narang, Jacob Devlin, Maarten Bosma, Gaurav Mishra, Adam Roberts, Paul Barham, Hyung Won Chung, Charles Sutton, Sebastian Gehrmann, Parker Schuh, Kensen Shi, Sasha Tsvyashchenko, Joshua Maynez, Abhishek Rao, Parker Barnes, Yi Tay, Noam M. Shazeer, Vinodkumar Prabhakaran, Emily Reif, Nan Du, Benton C. Hutchinson, Reiner Pope, James Bradbury, Jacob Austin, Michael Isard, Guy Gur-Ari, Pengcheng Yin, Toju Duke, Anselm Levskaya, Sanjay Ghemawat, Sunipa Dev, Henryk Michalewski, Xavier García, Vedant Misra, Kevin Robinson, Liam Fedus, Denny Zhou, Daphne Ippolito, David Luan, Hyeontaek Lim, Barret Zoph, Alexander Spiridonov, Ryan Sepassi, David Dohan, Shivani Agrawal, Mark Omernick, Andrew M. Dai, Thanumalayan Sankaranarayanan Pillai, Marie Pellat, Aitor Lewkowycz, Erica Moreira, Rewon Child, Oleksandr Polozov, Katherine Lee, Zongwei Zhou, Xuezhi Wang, Brennan Saeta, Mark Díaz, Orhan Firat, Michele Catasta, Jason Wei, Kathleen S. Meier-Hellstern, Douglas Eck, Jeff Dean, Slav Petrov, and Noah Fiedel. PaLM: Scaling language modeling with pathways. *ArXiv*, abs/2204.02311, 2022.
- [11] Marius Cordts, Mohamed Omran, Sebastian Ramos, Timo Rehfeld, Markus Enzweiler, Rodrigo Benenson, Uwe Franke, Stefan Roth, and Bernt Schiele. The cityscapes dataset for semantic urban scene understanding. *2016 IEEE Conference on Computer Vision and Pattern Recognition (CVPR)*, pages 3213–3223, 2016.
- [12] Ekin Dogus Cubuk, Barret Zoph, Jonathon Shlens, and Quoc V. Le. Randaugment: Practical automated data augmentation with a reduced search space. *2020 IEEE/CVF Conference on Computer Vision and Pattern Recognition Workshops (CVPRW)*, pages 3008–3017, 2019.
- [13] Tri Dao. Flashattention-2: Faster attention with better parallelism and work partitioning. *ArXiv*, abs/2307.08691, 2023.

- [14] Tri Dao, Daniel Y. Fu, Stefano Ermon, Atri Rudra, and Christopher Ré. Flashattention: Fast and memory-efficient exact attention with io-awareness. *ArXiv*, abs/2205.14135, 2022.
- [15] Ingrid Daubechies. *Ten Lectures on Wavelets*. Society for Industrial and Applied Mathematics, PHILADELPHIA, PENNSYLVANIA, 1992.
- [16] Mostafa Dehghani, Basil Mustafa, Josip Djolonga, Jonathan Heek, Matthias Minderer, Mathilde Caron, Andreas Steiner, Joan Puigcerver, Robert Geirhos, Ibrahim M. Alabdulmohsin, Avital Oliver, Piotr Padlewski, Alexey A. Gritsenko, Mario Luvcić, and Neil Houlsby. Patch n’ Pack: NaViT, a vision transformer for any aspect ratio and resolution. *ArXiv*, abs/2307.06304, 2023.
- [17] Alexey Dosovitskiy, Lucas Beyer, Alexander Kolesnikov, Dirk Weissenborn, Xiaohua Zhai, Thomas Unterthiner, Mostafa Dehghani, Matthias Minderer, Georg Heigold, Sylvain Gelly, Jakob Uszkoreit, and Neil Houlsby. An image is worth 16x16 words: Transformers for image recognition at scale. *ICLR*, 2021.
- [18] Patrick Esser, Robin Rombach, and Björn Ommer. Taming transformers for high-resolution image synthesis. *CVPR*, pages 12868–12878, 2021.
- [19] N. P. Jouppi et al. Ten lessons from three generations shaped google’s TPUv4i : Industrial product. In *Proceedings of the ACM/IEEE 48th Annual International Symposium on Computer Architecture*, ISCA ’21, Valencia, Spain, 2021.
- [20] M. Everingham, L. Van Gool, C.K. Williams, J. Winn, and A. Zisserman. The pascal visual object classes challenge. *International Journal of Computer Vision*, 2010.
- [21] A. Geiger, P. Lenz, and R. Urtasun. Are we ready for autonomous driving? the kitti vision benchmark suite. *IEEE Conference on Computer Vision and Pattern Recognition (CVPR)*, 2012.
- [22] Mor Geva, R. Schuster, Jonathan Berant, and Omer Levy. Transformer feed-forward layers are key-value memories. *ArXiv*, abs/2012.14913, 2020.
- [23] Rafael C. Gonzalez and Richard E. Woods. *Digital Image Processing 4th edition*. Pearson India, 2019.
- [24] I. J. Goodfellow, J. Shlens, and C. Szegedy. Explaining and Harnessing Adversarial Examples. *ArXiv e-prints*, 2014.
- [25] Geoffrey E. Hinton. How to represent part-whole hierarchies in a neural network. *ArXiv*, abs/2102.12627, 2021.
- [26] Jordan Hoffmann, Sebastian Borgeaud, Arthur Mensch, Elena Buchatskaya, Trevor Cai, Eliza Rutherford, Diego de Las Casas, Lisa Anne Hendricks, Johannes Welbl, Aidan Clark, et al. Training compute-optimal large language models. *arXiv preprint arXiv:2203.15556*, 2022.
- [27] Chao Jia, Yinfei Yang, Ye Xia, Yi-Ting Chen, Zarana Parekh, Hieu Pham, Quoc V. Le, Yun-Hsuan Sung, Zhen Li, and Tom Duerig. Scaling up visual and vision-language representation learning with noisy text supervision. In *International Conference on Machine Learning*, 2021.
- [28] Norm Jouppi, George Kurian, Sheng Li, Peter Ma, Rahul Nagarajan, Lifeng Nai, Nishant Patil, Suvinay Subramanian, Andy Swing, Brian Towles, Clifford Young, Xiang Zhou, Zongwei Zhou, and David A Patterson. Tpu v4: An optically reconfigurable supercomputer for machine learning with hardware support for embeddings. In *Proceedings of the 50th ACM/IEEE Annual International Symposium on Computer Architecture*, ISCA ’23, Orlando, FL, USA, 2023.
- [29] Nikita Kitaev, Lukasz Kaiser, and Anselm Levskaya. Reformer: The efficient transformer. *ArXiv*, abs/2001.04451, 2020.
- [30] Taku Kudo and John Richardson. SentencePiece: A simple and language independent subword tokenizer and detokenizer for neural text processing. In *Conference on Empirical Methods in Natural Language Processing*, 2018.
- [31] Kenton Lee, Mandar Joshi, Iulia Turc, Hexiang Hu, Fangyu Liu, Julian Eisenschlos, Urvashi Khandelwal, Peter Shaw, Ming-Wei Chang, and Kristina Toutanova. Pix2Struct: Screenshot parsing as pretraining for visual language understanding. *ArXiv*, abs/2210.03347, 2022.
- [32] Ze Liu, Han Hu, Yutong Lin, Zhuliang Yao, Zhenda Xie, Yixuan Wei, Jia Ning, Yue Cao, Zheng Zhang, Li Dong, et al. Swin Transformer V2: Scaling Up Capacity and Resolution. *CVPR*, 2022.

- [33] Shangzhen Luan, Chen Chen, Baochang Zhang, J. Han, and Jianzhuang Liu. Gabor convolutional networks. *IEEE Winter Conference on Applications of Computer Vision (WACV)*, pages 1254–1262, 2018.
- [34] Minesh Mathew, Viraj Bagal, Rubèn Pérez Tito, Dimosthenis Karatzas, Ernest Valveny, and C.V. Jawahar. Infographicvqa. *2022 IEEE/CVF Winter Conference on Applications of Computer Vision (WACV)*, pages 2582–2591, 2021.
- [35] Sandip Mazumder. *Numerical Methods for Partial Differential Equations: Finite Difference and Finite Volume Methods 1st Edition*. Academic Press, 2015.
- [36] Charlie Nash, Jacob Menick, Sander Dieleman, and Peter W. Battaglia. Generating images with sparse representations. *ArXiv*, abs/2103.03841, 2021.
- [37] Niki Parmar, Ashish Vaswani, Jakob Uszkoreit, Lukasz Kaiser, Noam Shazeer, Alexander Ku, and Dustin Tran. Image transformer. *ArXiv*, abs/1802.05751, 2018.
- [38] Alec Radford, Jong Wook Kim, Chris Hallacy, Aditya Ramesh, Gabriel Goh, Sandhini Agarwal, Girish Sastry, Amanda Askell, Pamela Mishkin, Jack Clark, et al. Learning transferable visual models from natural language supervision. In *ICML*, pages 8748–8763, 2021.
- [39] Colin Raffel, Noam M. Shazeer, Adam Roberts, Katherine Lee, Sharan Narang, Michael Matena, Yanqi Zhou, Wei Li, and Peter J. Liu. Exploring the limits of transfer learning with a unified text-to-text transformer. *ArXiv*, abs/1910.10683, 2019.
- [40] Aditya Ramesh, Mikhail Pavlov, Gabriel Goh, Scott Gray, Chelsea Voss, Alec Radford, Mark Chen, and Ilya Sutskever. Zero-shot text-to-image generation. *ArXiv*, abs/2102.12092, 2021.
- [41] Tomer Ronen, Omer Levy, and Avram Golbert. Vision transformers with mixed-resolution tokenization. *2023 IEEE/CVF Conference on Computer Vision and Pattern Recognition Workshops (CVPRW)*, pages 4613–4622, 2023.
- [42] Aurko Roy, M. Saffar, Ashish Vaswani, and David Grangier. Efficient content-based sparse attention with routing transformers. *ArXiv*, abs/2003.05997, 2020.
- [43] Olga Russakovsky, Jia Deng, Hao Su, Jonathan Krause, Sanjeev Satheesh, Sean Ma, Zhiheng Huang, Andrej Karpathy, Aditya Khosla, Michael Bernstein, Alexander C. Berg, and Li Fei-Fei. Imagenet large scale visual recognition challenge. *IJCV*, pages 1–42, 2014.
- [44] Jaydip Sen and Subhasish Dasgupta. Adversarial attacks on image classification models: Fgsm and patch attacks and their impact. *ArXiv*, abs/2307.02055, 2023.
- [45] G. D. Smith. *Numerical Solution of Partial Differential Equations: Finite Difference Methods (Oxford Applied Mathematics and Computing Science Series) 3rd Edition*. Clarendon Press, 1986.
- [46] Xinying Song, Alexandru Salcianu, Yang Song, Dave Dopson, and Denny Zhou. Fast Word-Piece tokenization. In *Conference on Empirical Methods in Natural Language Processing*, 2020.
- [47] Andreas Steiner, Alexander Kolesnikov, , Xiaohua Zhai, Ross Wightman, Jakob Uszkoreit, and Lucas Beyer. How to train your vit? data, augmentation, and regularization in vision transformers. *arXiv preprint arXiv:2106.10270*, 2021.
- [48] Gilbert Strang and Truong Nguyen. *Wavelets and Filter Banks*. Wellesley-Cambridge Press, 1996.
- [49] Yi Tay, M. Dehghani, Dara Bahri, and Donald Metzler. Efficient transformers: A survey. *ArXiv*, abs/2009.06732, 2020.
- [50] Yi Tay, Mostafa Dehghani, Vinh Q. Tran, Xavier García, Jason Wei, Xuezhi Wang, Hyung Won Chung, Dara Bahri, Tal Schuster, Huaixiu Steven Zheng, Denny Zhou, Neil Houlsby, and Donald Metzler. UL2: Unifying language learning paradigms. In *ICLR*, 2022.
- [51] Yi Tay, Vinh Q. Tran, Sebastian Ruder, Jai Gupta, Hyung Won Chung, Dara Bahri, Zhen Qin, Simon Baumgartner, Cong Yu, and Donald Metzler. Charformer: Fast character transformers via gradient-based subword tokenization. *ArXiv*, abs/2106.12672, 2021.
- [52] Chunwei Tian, Menghua Zheng, Wangmeng Zuo, Bob Zhang, Yanning Zhang, and David Zhang. Multi-stage image denoising with the wavelet transform. *Pattern Recognit.*, 134:109050, 2022.

- [53] Hugo Touvron, Matthieu Cord, and Hervé Jégou. DeiT III: Revenge of the ViT. In *ECCV*, 2022.
- [54] Aäron van den Oord, Oriol Vinyals, and Koray Kavukcuoglu. Neural discrete representation learning. *ArXiv*, abs/1711.00937, 2017.
- [55] Ashish Vaswani, Prajit Ramachandran, A. Srinivas, Niki Parmar, Blake A. Hechtman, and Jonathon Shlens. Scaling local self-attention for parameter efficient visual backbones. *CVPR*, pages 12889–12899, 2021.
- [56] Ashish Vaswani, Noam Shazeer, Niki Parmar, Jakob Uszkoreit, Llion Jones, Aidan N Gomez, Łukasz Kaiser, and Illia Polosukhin. Attention is all you need. In *Advances in neural information processing systems*, pages 5998–6008, 2017.
- [57] Fu Wang and Tariq Alkhalifah. Learnable gabor kernels in convolutional neural networks for seismic interpretation tasks. *ArXiv*, abs/2308.05202, 2023.
- [58] Sinong Wang, Belinda Z. Li, Madian Khabsa, Han Fang, and Hao Ma. Linformer: Self-attention with linear complexity. *ArXiv*, abs/2006.04768, 2020.
- [59] Linting Xue, Aditya Barua, Noah Constant, Rami Al-Rfou, Sharan Narang, Mihir Kale, Adam Roberts, and Colin Raffel. ByT5: Towards a token-free future with pre-trained byte-to-byte models. *Transactions of the Association for Computational Linguistics*, 10:291–306, 2021.
- [60] Ting Yao, Yingwei Pan, Yehao Li, Chong-Wah Ngo, and Tao Mei. Wave-vit: Unifying wavelet and transformers for visual representation learning. In *ECCV*, 2022.
- [61] Hongxu Yin, Arash Vahdat, José Manuel Álvarez, Arun Mallya, Jan Kautz, and Pavlo Molchanov. A-vit: Adaptive tokens for efficient vision transformer. *CVPR*, pages 10799–10808, 2022.
- [62] Jiahui Yu, Xin Li, Jing Yu Koh, Han Zhang, Ruoming Pang, James Qin, Alexander Ku, Yuanzhong Xu, Jason Baldridge, and Yonghui Wu. Vector-quantized image modeling with improved vqgan. *ICLR*, 2022.
- [63] Jiahui Yu, Zirui Wang, Vijay Vasudevan, Legg Yeung, Mojtaba Seyedhosseini, and Yonghui Wu. Coca: Contrastive captioners are image-text foundation models. *Trans. Mach. Learn. Res.*, 2022, 2022.
- [64] Manzil Zaheer, Guru Guruganesh, Kumar Avinava Dubey, Joshua Ainslie, Chris Alberti, Santiago Ontañón, Philip Pham, Anirudh Ravula, Qifan Wang, Li Yang, and Amr Ahmed. Big bird: Transformers for longer sequences. *ArXiv*, abs/2007.14062, 2020.
- [65] Xiaohua Zhai, Alexander Kolesnikov, Neil Houlsby, and Lucas Beyer. Scaling vision transformers. *CVPR*, pages 1204–1213, 2022.
- [66] Hongyi Zhang, Moustapha Cissé, Yann Dauphin, and David Lopez-Paz. mixup: Beyond empirical risk minimization. *ArXiv*, abs/1710.09412, 2017.
- [67] Bolei Zhou, Hang Zhao, Xavier Puig, Sanja Fidler, Adela Barriuso, and Antonio Torralba. Semantic understanding of scenes through the ade20k dataset. *International Journal of Computer Vision*, 127:302 – 321, 2016.
- [68] Zhenhai Zhu and Radu Soricut. H-transformer-1d: Fast one-dimensional hierarchical attention for sequences. In *Annual Meeting of the Association for Computational Linguistics*, 2021.